



HAL
open science

Characterization of a highly neutralizing single monoclonal antibody to botulinum neurotoxin type A

Sébastien Brier, Christine Rasetti-Escargueil, Anne Wijkhuisen, Stéphanie Simon, Maud Marechal, Emmanuel Lemichez, Michel Popoff

► To cite this version:

Sébastien Brier, Christine Rasetti-Escargueil, Anne Wijkhuisen, Stéphanie Simon, Maud Marechal, et al.. Characterization of a highly neutralizing single monoclonal antibody to botulinum neurotoxin type A. *FASEB Journal*, 2021, 35 (5), 10.1096/fj.202002492R . pasteur-03254500

HAL Id: pasteur-03254500

<https://pasteur.hal.science/pasteur-03254500v1>

Submitted on 8 Jun 2021

HAL is a multi-disciplinary open access archive for the deposit and dissemination of scientific research documents, whether they are published or not. The documents may come from teaching and research institutions in France or abroad, or from public or private research centers.

L'archive ouverte pluridisciplinaire **HAL**, est destinée au dépôt et à la diffusion de documents scientifiques de niveau recherche, publiés ou non, émanant des établissements d'enseignement et de recherche français ou étrangers, des laboratoires publics ou privés.



Distributed under a Creative Commons Attribution - NonCommercial 4.0 International License

33 mechanism of TA12 and emphasizes on the potential of using single mAbs for the treatment of
34 botulism type A.

35

36 **Key Words**

37 Botulinum neurotoxin; Botulism; Monoclonal antibody; Synaptic vesicle protein 2; GT1b,
38 Mass spectrometry; Hydrogen-Deuterium eXchange; Epitope mapping

39

40 **Running title**

41 Potent neutralization of BoNT/A1 with a single mAb

42

43 **Nonstandard abbreviations**

44 BoNT, botulinum neurotoxin

45 L, light chain

46 H, heavy chain

47 H_C, half C-terminal H chain

48 H_N, half N-terminal H chain

49 SV2C, synaptic vesicle protein 2C

50 gSV2C, glycosylated SV2C

51 SNARE, soluble *N*-ethylmaleimide-sensitive-factor attachment protein receptor

52 mAb, monoclonal antibody

53 HDX-MS, Hydrogen/Deuterium eXchange Mass Spectrometry

54 TCEP, Tris(2-carboxylethyl)phosphine

55 EIA, enzyme immunoassay

56 LD, luminal domain

57 BSA, bovine serum albumin

58 AMC, anti-mouse Fc

59 TGY, trypticase-glucose-yeast extract

60 VHH, variable domain of heavy chain

61 MLD, mouse lethal dose

62

63 INTRODUCTION

64 Botulism is a rare but severe disease that results from botulinum neurotoxin (BoNT)
65 intoxication. Naturally acquired botulism can develop in three main forms: foodborne BoNT
66 intoxication, intestinal colonization by BoNT-producing clostridium (infant botulism and more
67 rarely botulism by intestinal colonization in adults), or wound botulism. Among the seven
68 different BoNT toxinotypes, BoNT/A is the most potent toxin with a lethal dose for human
69 estimated at ~1 ng/kg by parenteral route (1, 2). BoNTs and specially the BoNT/A toxinotype
70 are therefore classified by the Centers for Diseases Control and Prevention (CDC) among the
71 six major bioterrorism agents (category A) (3). BoNT/A is a ~1296 residues long protein that
72 is proteolytically processed into a light (L) and a heavy chain (H) linked by a single disulfide
73 bond. The L chain contains the intracellularly active enzymatic site that specifically cleaves
74 neuronal members of the *N*-ethylmaleimide sensitive factor attachment protein receptors
75 (SNAREs) complex required for the release of acetylcholine. The C-terminal H chain (H_C)
76 recognizes both the intraluminal loop of the synaptic vesicle glycoprotein 2C (SV2C) and
77 GT1b/GD1a gangliosides as functional dual receptors on neuronal cells. Finally, the N-terminal
78 H domain (H_N) is involved in the translocation of the L chain from endocytic vesicles into the
79 cytosol of neuronal cell targets (4-11).

80 Antitoxin serotherapies are currently the only specific and available treatments for
81 botulism. The clinical benefit and effectiveness of such therapies remain however linked to
82 their use at the early onset of the disease *only*. The equine antitoxin therapy composed of
83 polyclonal IgG antibodies is the most available treatment although it is often associated to
84 hypersensitivity reactions including serum sickness and cardiac arrest (12, 13). Human
85 botulism-immune globulins from vaccinated donors have been developed notably for the
86 treatment of infant botulism (14). The first one—BabyBIG, is supplied by the California
87 Department of Public Health, but with limited stock. This formulation has been recently
88 discontinued and will be replaced with a new formulation currently under clinical development
89 (15). Recently, the safety of a new cocktail composed of three humanized mAbs (XOMA 3B)
90 engineered to neutralize BoNT/A subclasses has been evaluated and confirmed in healthy
91 volunteers (16). The European AntiBotABE Program has allowed the isolation of recombinant
92 humanized antibodies neutralizing BoNT/A, B and E. Protective antibody combinations against
93 BoNT/A and BoNT/B showed cross-neutralization of both BoNT/A1 and A2 as well as
94 BoNT/B1 and B2, respectively (17).

95 Monoclonal antibodies (mAbs) represent therefore a promising alternative strategy to treat
96 botulism with the advantage of being better tolerated by patients and produced in a more

97 reproducible and safer way than animal hyperimmune serum. Various murine or humanized
98 mAbs raised against whole BoNTs or BoNT subdomains have been evaluated for their
99 neutralizing potency and their possible therapeutic use (review in (17, 18)). Most often, efficient
100 toxin neutralization requires a combination of several mAbs. For example, the association of
101 three mAbs has been reported to neutralize BoNT/A, BoNT/E, or BoNT/F, respectively (19-
102 21). Recently, a single anti-BoNT/A tri-epitopic mAb with equivalent binding and
103 neutralization potency than three distinct mAbs has been generated (22). The use of a single
104 mAb as alternative therapeutic antitoxin agent appears therefore promising and offers the
105 advantage to simplify the process of development and to reduce the cost of production.

106 We previously reported a potent neutralizing murine mAb (named TA12) generated against
107 the C-terminal domain of the BoNT/A1 heavy chain (H_CA1) (23, 24). In this study, we focused
108 on the structural characterization of the TA12:H_CA1 complex by Hydrogen/Deuterium
109 eXchange Mass Spectrometry (HDX-MS) approach combined with site directed mutagenesis
110 and functional assays (25, 26). We report that TA12 targets a conformational epitope on H_CA1
111 located at the junction between the H_{CC} and the H_{CN} subdomains. The TA12 epitope overlaps
112 with both the SV2C cell receptor and the GT1b binding sites, hence perturbing the dual-receptor
113 binding process required for the entry of BoNT/A1 into neuronal cells.

114

115 **MATERIALS AND METHODS**

116 **Biological reagents**

117 mAb TA12 was prepared and affinity purified on protein A beads (Prosep-A High capacity,
118 Millipore, Billerica, USA) as previously described (27).

119 Recombinant H_C of BoNT/A1 (H_CA1), corresponding to the receptor binding domain of
120 BoNT/A1 was prepared as previously described (28). DNAs encoding H_C of BoNT/A subtypes
121 were PCR amplified with primers and *C. botulinum* genomic DNA (**Extended Table 1**) and
122 cloned into pET28a. Recombinant H_C containing N-terminal 6xHis-tag were produced and
123 purified as previously described (28). Primers used to generate H_CA1 mutants are indicated in
124 **Extended Table 2**.

125 cDNA encoding the human intraluminal SV2C fragment L4 (amino acid 454 to 579,
126 hereafter named SV2C-LD) was PCR amplified as previously described (29). Briefly, DNA
127 encoding the amino acids 454 to 579 of human SV2C was PCR amplified with primers P1415
128 (5'- GGATCCTTCCCTGATGTCATTAAACCTCTG-3') and P1416 (5'-
129 GAATTCCTAGTAGGCACTATAGTCATCATCAAA-3') adding *Bam*HI and *Eco*RI
130 restriction sites, respectively, and was cloned into pGEX-2T at the corresponding restriction

131 sites. The construction was verified by DNA sequencing. The fusion protein (41 kDa) contains
132 N-terminal GST and C-terminal SV2C-LD linked by Gly-Ser resulting from the *Bam*HI site.
133 The recombinant plasmid was cloned into *E. coli* BL21 DE3 and the resulting bacterial strain
134 was grown in LB medium containing ampicillin (100 µg/ml). The culture was induced with
135 IPTG (0.2 mM) and further grown at 18°C for 18 h. The bacterial cells were washed with
136 distilled water, suspended in 50 mM Tris, 150 mM NaCl, 10 mM MgCl₂, 1 mM dithiothreitol,
137 0.1% Tween20 containing complete protease inhibitor cocktail EDTA free (Roche, France),
138 and lysed by ultrasonication. The lysate was incubated with Glutathione-Sepharose-4B beads
139 (GE Healthcare) for 1 h at 4°C. The beads were washed three times with the same buffer and a
140 50% suspension in the same buffer was used for the pull-down assays.

141 For HDX-MS experiments, 6His-tag-SV2C-LD was used. The PCR amplified DNA
142 encoding SV2C-LD was cloned into pET28 vector at the *Bam*HI-*Eco*RI site. The recombinant
143 N-terminal 6His-tag-SV2C-LD protein was produced in *E. coli* BL21 DE3 and purified on a
144 Talon metal affinity matrix (Clontech) equilibrated in 10 mM Tris, 150 mM NaCl, 10 mM
145 imidazole, 10 mM TCEP, pH 7.5. The recombinant protein was eluted with the same buffer
146 supplemented with 100 mM imidazole and dialyzed against the same buffer without imidazole.
147

148 **Affinity determination of mAb TA12**

149 The affinities of mAb TA12 for different recombinant HcBoNT isoforms were determined
150 by Bio-layer Interferometry using the ForteBio system (Pall Laboratory). mAb TA12 prepared
151 at 10 µg/mL in EIA (enzyme immunoassay) buffer (0.1 M phosphate buffer, pH 7.4, 0.15 M
152 NaCl, 0.1% BSA, and 0.01% sodium azide) + 0.02% Tween 20 (Sigma) was dispensed in 96-
153 well microplates at a volume of 200 µL per well. The same concentration occupied 8 vertical
154 wells. In other wells, recombinant HcBoNT proteins were dispensed at 8 titrated concentrations
155 (between 100 and 0 nM depending on the protein). A glycine (Sigma, pH [1.4]) regeneration
156 solution and EIA buffer + 0.02% Tween 20 for baseline stabilization and neutralization was
157 also prepared. The plate was agitated at 1000 rpm over the entire course of the experiment.
158 Prior to the binding measurements, the anti-mouse Fc (AMC) sensors tips were hydrated in EIA
159 buffer + 0.02% tween 20. The sensor tips were then transferred to the EIA buffer + 0.02%
160 Tween 20 for the baseline, then for 300 sec into wells containing mAb for loading step. After
161 baseline step in EIA buffer + 0.02% Tween 20 for 60 sec, the binding kinetics were measured
162 by dipping the mAb-coated sensors into the wells containing recombinant HcBoNT at varying
163 concentrations. The binding interactions were monitoring over a 900 sec associated period and
164 followed by a 900 sec dissociation period in the wells containing EIA buffer +0.02 % Tween

165 20. Between each binding cycle, the AMC sensors tips were regenerated with wells containing
166 glycine and neutralized in the EIA buffer + 0.02% tween 20. The equilibrium dissociation
167 constant (K_D) was calculated using the ratio between the dissociation rate constant (k_{off}) and
168 the association rate constant (k_{on}), obtained with a global Langmuir 1:1 fit (Octet Data Analysis
169 software, vHT.10).

170

171 **GST pull down assay**

172 Recombinant SV2C-LD immobilized on glutathione-Sepharose-4B matrix (GE healthcare,
173 France) (30 μ L of 50% bead suspension) was incubated for 90 min at 4°C with H_CA1 solutions
174 prepared with or without mAb TA12 in 50 mM Tris buffer, 150 mM NaCl, 10 mM MgCl₂, 2
175 mM dithiothreitol, 0.1% Tween 20, pH 7.5, supplemented with antiproteases (protease inhibitor
176 cocktail EDTA free, Roche Diagnostics, Germany) (final volume 400 μ L). H_CA1:TA12
177 solutions were pre-incubated for 15 min at room temperature before use. Beads were collected
178 by centrifugation and washed three times with the same buffer. Washed pellets were suspended
179 in SDS/2-mercaptoethanol sample buffer for 2 min at 95°C and analyzed by SDS-PAGE.
180 Proteins were stained by Coomassie blue.

181

182 **Ganglioside binding assay**

183 Binding of H_CA1 to the GT1b ganglioside was assessed in a solid phase assay as
184 previously described (30-32). Briefly, bovine brain GT1b (Calbiochem, France) stored in
185 dimethyl sulfoxide (20 mg/mL) at -20°C was diluted in methanol and applied overnight to 96-
186 well plates (Corning-Costar, France) at 2 μ g per well. Methanol was evaporated at room
187 temperature and the plates were washed three times with phosphate-buffered saline containing
188 0.05 % Tween 20 (Sigma, France) (PBST). Plates were blocked with 5% non-fat skim milk in
189 PBST for 1 h at room temperature and washed with PBST. H_CA1 was then dispensed (10
190 nM/well in PBS) in the control wells and incubated for 2 h at 4°C. For competition with mAb
191 TA12, H_CA1 (10 nM) was incubated with various concentrations of TA12 in 100 μ L PBS for
192 15 min at room temperature prior being applied to GT1b coated wells for 2 h at 4°C. After
193 washing with PBST, bound H_CA1 was detected with rabbit anti-H_CA1 (1:10,000) (29) and horse
194 radish peroxidase (HRP) goat anti-rabbit immunoglobulin IgG (1:3,000) (Invitrogen, France).
195 Ortho phenyldiamine (Sigma, France) was used as substrate (1 mg/mL in citrate buffer pH
196 4.5 containing H₂O₂), and the reaction was stopped with HCl 3 M (50 μ L/well). The extinction
197 was measured at 490 nm and 650 nm as reference.

198

199 **Neutralizing activity**

200 BoNTs were prepared from *C. botulinum* cultures in TGY (trypticase-glucose-yeast
201 extract) medium for four days under anaerobic conditions at 37°C as previously described (33).
202 Briefly, the cultures were acidified at pH 3.5 with sulfuric acid, centrifuged at 10,000 x g for
203 15 min at 4°C, washed with distilled water, and the BoNT complexes were extracted three times
204 with 0.2 M phosphate buffer pH 6.3. BoNT complexes were precipitated with 65% ammonium
205 sulfate saturation and then dialyzed against 50 mM phosphate buffer, pH 6.3 containing 0.2%
206 gelatin (PB-G).

207 Mouse protection assay was performed with male Swiss mice (Charles River) weighing
208 20-22 g as previously described (34). Variable amounts of TA12 were incubated with 5
209 estimated mouse 50% lethal doses of either BoNT/A1, A2, A3, A5 or A7 in PB-G for 30 min
210 at room temperature. The mixtures (0.5 mL) were then injected intraperitoneally into mice with
211 control mice receiving BoNT alone. Mice were observed and any death was recorded every day
212 during 4 days.

213

214 **Ethic statements**

215 All experiments were performed in accordance with French and European Community
216 guidelines for laboratory animal handling. The protocols of experiments were approved by
217 Institut Pasteur CETEA (Comité d'Ethique en Expérimentation Animale) with the agreement
218 of laboratory animal use (N° 2013-0116) and by the Ministère de l'Education Nationale et de
219 l'Enseignement Supérieur with the agreement 02026.02.

220

221 **HDX-MS experiments**

222 A summary of the HDX data containing the main experimental details is provided in
223 **Extended Table 3** (35). Prior to initiating the labeling, the quality of each protein was assessed
224 by SDS-PAGE and intact mass analysis (**Extended Figure 1**).

225

226 **Sample preparation.** For epitope mapping, H_CA1 was labeled in both the presence and absence
227 of the mouse mAb TA12. The TA12: H_CA1 complex was formed by mixing 3 µL of H_CA1 (29
228 µM in buffer A: 10 mM Tris, 150 mM NaCl, pH 7.4) with 4.5 µL of mAb TA12 (27 µM in
229 buffer A). Control samples (unbound H_CA1) were prepared in parallel by replacing TA12 with
230 buffer A. After 1 h incubation at 20°C, the labeling was initiated by adding 67.5 µL of

231 deuterated buffer (10 mM Tris, 150 mM NaCl, pD 7.4; D₂O/H₂O ratio: 90/10%). Assuming a
232 K_D value of ~20 pM (24) (and this study), ~100% of H_CA1 remains bound to TA12 during
233 hydrogen exchange. Continuous labeling was performed at 20°C for t = 0.16, 1, 5, 10, 30, 60
234 and 120 min. Aliquots of 10 μL (*i.e.*, 11.6 pmoles of H_CA1) were removed and quenched upon
235 mixing with 50 μL of an ice cold solution of 2% formic acid, 4M urea to decrease the pH to 2.5
236 (Final D₂O/H₂O ratio: 15/85%). Quenched samples were immediately snap frozen in liquid
237 nitrogen and stored at -80°C until MS acquisition (less than 3 days).

238 An identical procedure was used to map the SV2C-LD interaction site on H_CA1. The
239 SV2C-LD: H_CA1 complex was formed by mixing 3 μL of H_CA1 (29 μM in buffer A) with 4.5
240 μL of SV2C-LD (22 μM in buffer A supplemented with 10 mM TCEP). The labeling was
241 performed in the presence of 1 mM TCEP at 20°C. Assuming a K_D value of 28 nM (6), 90.5%
242 of H_CA1 remains bound to SV2C-LD during labeling.

243 Undeuterated H_CA1 samples were obtained following the same experimental procedure. A
244 fully deuterated H_CA1 control was prepared in 10 mM Tris buffer, 150 mM NaCl, 8 M urea-
245 d₄, pD 7.4 (D₂O/H₂O ratio: 90/10%), incubated overnight at 20°C and processed as described
246 above. All samples were prepared in triplicate for each time point and condition (independent
247 technical replicate).

248
249 **Data acquisition.** Quenched samples were rapidly thawed and injected onto a nanoACQUITY
250 UPLC M-Class system (Waters Corporation, Milford, MA) equipped with a HDX manager
251 maintained at 0°C to minimize back-exchange. Labeled samples (9.7 pmol of H_CA1 either alone
252 or with 13.5/11 pmol of TA12/SV2C-LD) were digested using an in-house packed cartridge
253 (2.0 x 20 mm, 63 μL bed volume) of immobilized pepsin beads (Thermo Scientific, Rockford,
254 IL) for 2 min at 20°C. Peptides were directly trapped and desalted onto a C18 Trap column
255 (VanGuard BEH 1.7 μm, 2.1 x 5 mm, Waters Corporation, Milford, MA) at a flow rate of 100
256 μL/min (0.15% formic acid) and separated by a 10 min linear gradient of 5-40% acetonitrile at
257 40 μL/min using an ACQUITY UPLC BEH C18 analytical column (1.7 μm, 1 × 100 mm,
258 Waters Corporation, Milford, MA). After each run, the pepsin column was manually cleaned
259 with two consecutive injections of 1% formic acid, 5% acetonitrile, 1.5 M guanidinium
260 chloride, pH 1.7. Blank injections were performed between each run to confirm the absence of
261 carry-over. Mass spectra were acquired in resolution and positive mode (*m/z* 50-2000) on a
262 Synapt G2-Si HDMS mass spectrometer (Waters Corporation, Milford, MA) equipped with a
263 standard ESI source and lock-mass correction. Peptic peptides were identified in undeuterated

264 samples by a combination of data independent acquisition (MS^E) and exact mass measurement
265 (below 5.0 ppm mass error) using the same chromatographic conditions than for the deuterated
266 samples.

267

268 **Data processing.** The initial peptide map of HcA1 was generated by database searching in
269 ProteinLynX Global server 3.0 (Waters corporation, Milford, MA) using the following
270 processing and workflow parameters: low and elevated intensity thresholds set to 100.0 and
271 50.0 counts; intensity threshold sets to 750.0 counts; automatic peptide and fragment tolerance;
272 non-specific primary digest reagent; false discovery rate sets to 4%. Each fragmentation
273 spectrum was manually inspected for assignment confirmation. The peptide map was refined
274 in DynamX 3.0 (Waters corporation, Milford, MA) using the following Import PLGS results
275 filter: minimum intensity = 1500; minimum products per amino acid = 0.4; minimum score =
276 6.8; maximum MH⁺ error (ppm) = 5; file threshold = 2.

277 DynamX 3.0 was used to extract the centroid masses of all peptides selected for HDX-MS
278 analyses. Only one unique charge state was considered per peptide and no back-exchange
279 correction was performed. HDX results are reported as relative deuterium exchange level
280 expressed in either mass unit or fractional exchange. Fractional exchange data were calculated
281 by dividing the experimental uptake value by the theoretically maximum number of
282 exchangeable backbone amide hydrogens that could be replaced into each peptide in 90%
283 excess deuterium. MEMHDX (36) was used to visualize and statistically validate the HDX data
284 (Wald test, false discovery rate of 5%).

285 The presence of bimodal *m/z* envelopes (i.e., EX1 behavior) was determined by visually
286 inspecting the shape of the isotopic distribution for all peptides. HX-Express2 software was
287 used to extract the uptake value of bimodal *m/z* envelopes using a Double-Gaussian fitting (37).

288

289 RESULTS

290 TA12 efficiently neutralizes BoNT/A1

291 BoNT/A is divided into 8 distinct subtypes (BoNT/A1 to BoNT/A8) according to their
292 amino acid sequence variations ranging from 2.9 % to 15.6 % (1). Although the BoNT/A
293 toxinotype is defined by its neutralization with polyclonal anti-BoNT/A antibodies, each
294 subtype can be distinctly neutralized by individual mAbs (1). We recorded that TA12 efficiently
295 neutralized BoNT/A1 and displayed an inhibitory spectrum on BoNT/A subtypes A2, A3, and
296 A7 (**Table 1**) (23). However, it showed a weak neutralizing activity against BoNT/A5 (**Table**
297 **1**). Taken together, these results confirm that TA12 is a highly neutralizing mAb of the most

298 potent subtype BoNT/A1 with medium neutralizing activity against BoNT/A2 and A3 subtypes
299 and low neutralizing activity against BoNT/A5 (38, 39).

300

301 **TA12 binding affinity to BoNT/A subtypes**

302 TA12 binding affinity to the H_C domain of different BoNT/A subtypes was determined by
303 Bio-Layer Interferometry. The binding affinity of TA12 was very high for H_CA1, H_CA2, and
304 H_CA3 with K_D values in the low pM range (i.e., < 100 pM; **Table 2**) in good agreement with
305 previous data obtained for H_CA1 using Biacore instrument (24). The TA12 affinity was slightly
306 lower with H_CA2 and significantly reduced with H_CA4, H_CA5, and H_CA7 with K_D values in the
307 low nM range. These differences in K_D mainly result from faster dissociation rate values for
308 H_CA2, H_CA4, H_CA5, and H_CA7 as compared to H_CA1. Indeed, TA12 interacts with the H_C
309 domain of the different BoNT/A subtypes with similar on-rates values (**Table 2**). Consistent
310 with the protection of TA12 on BoNT/A subtypes, TA12 binds BoNT/A H_C domains with
311 maximal affinities for BoNT/A1, A2, and A3. These results reveal that low picomolar affinities
312 for the H_C domain are required to achieve maximal TA12 neutralizing power in the mouse
313 lethality assay.

314

315 **TA12 recognizes a conformational epitope at the junction between the H_{CC} and the H_{CN}** 316 **subdomains of H_CA1**

317 To better understand the mechanism underlying BoNT/A1 neutralization by TA12, the free
318 and TA12-bound state of H_CA1 were subjected to HDX-MS analysis. The quench and pepsin
319 digestions were first optimized to generate a peptide map with high sequence coverage and
320 peptide redundancy. Urea was included in the quench buffer to favor the dissociation of the
321 TA12: H_CA1 complex and increase the accessibility of both proteins to pepsin during the
322 digestion step. A total of 98 unique peptides covering 85.2% of the H_CA1 sequence were
323 confidently identified, of which 62 were selected for HDX-MS (**Extended Figure 2**).
324 Overlapping peptides were only used to increase the spatial resolution when their back-
325 exchange values were similar (i.e., < 10%; **Extended file HDX.xls**).

326 The binding of TA12 reduces the solvent accessibility of 12 peptides covering six distinct
327 regions within H_CA1 (**Figure 1A, Extended Figure 3**). The main decreases in solvent
328 accessibility occur in region 2 (peptide 1005-1016; loop β31-β32, β32), in region 4 (peptides
329 1114-1134, 1115-1134, 1116-1134 and 1117-1134; loop-β38-loop), and in region 5 (peptides
330 1135-1144, 1135-1147 and 1148-1154; β39-loop-β40-loop-β41). Inspection of the different

331 overlapping peptides in regions 2 and 4 reveals that the reduction of solvent accessibility is
332 restricted to segments 1005-1009 and 1116-1124. In addition, a slight but statistically
333 significant reduction in solvent accessibility was observed in region 1 (peptides 946-955, 946-
334 958 and 946-961; loop β 27- β 28) and in region 6 (peptide 1250-1261; β 49-loop) (**Figure 1A**
335 **and Extended Figure 4A**).

336 As shown in **Figure 1B**, TA12 binds H_CA1 at the junction between the N-terminal lectin
337 subdomain (H_{CN}) and the C-terminal trefoil subdomain (H_{CC}). The TA12 epitope appears
338 conformational and mainly formed by the β 27- β 28 and β 31- β 32 loops of H_{CN} and by the
339 structural elements β 38 to β 41, β 49 and the β 37- β 38, β 39- β 40, β 40- β 41 and β 49- β 50 loops of
340 H_{CC}. Interestingly, the HDX-MS defined TA12 epitope contains elements identified as
341 important for the binding of both the SV2C luminal domain (SV2C-LD) and the GT1b
342 ganglioside (**Figure 1B, regions 4, 5 and 6**). Indeed, the SV2C-LD binding site has been
343 characterized in the H_{CN}-H_{CC} interface and the ganglioside binding pocket in the C-terminal
344 part of H_{CC} (Glu1203-Gly1279 with Tyr1117 and Phe1252 playing a critical role) (6, 9, 40).
345 Finally, TA12 also increases the deuterium uptake in region 3 (peptide 1017-1035; β 32-loop-
346 β 33) in the lectin subdomain (**Figures 1A, 1B**). Upon complex formation, the isotopic profile
347 of peptide 1017-1035 adopts a bimodal distribution characterized by a low and high m/z protein
348 population (**Figure 1C**). Bimodal isotopic patterns result from cooperative exchanges (also
349 known as EX1 regime) and are very rare in proteins under physiological conditions. Several
350 experimental factors, such as carry-over or abnormal gas-phase back-exchange are known to
351 generate false EX1 signatures. To rule out these possibilities, a blank was acquired between
352 each injection and the pepsin column was carefully washed after each run. In addition, specific
353 settings were applied on the mass spectrometer (source and ion transfer) to prevent gas-phase
354 deuterium loss (41). We are therefore confident that the bimodal pattern observed with peptide
355 1017-1035 is not an experimental artefact but a true change in dynamics imposed by the binding
356 of TA12. To extract the deuterium uptake level of the low and high m/z protein populations, the
357 bimodal isotopic envelop was fitted with two Gaussians. The low m/z population showed no
358 difference in deuterium uptake compared to free H_CA1 (**Figure 1C**). The high m/z population
359 however displayed an evident and constant increase in deuterium uptake over time, with the
360 incorporation of four additional deuteriums. This data confirms that segment 1017-1035 is
361 destabilized in the complex.

362 Taken together, these data reveal that TA12 targets a conformational epitope located at the
363 junction between the H_{CN} and H_{CC} subdomains that overlaps with the the SV2C-LD and the

364 GT1b binding site. The formation of the complex triggers a conformational change in the H_{CN}
365 domain that was not observed with the two previously described neutralizing antibodies ciA-
366 C2 and CR1 (see discussion) (42-45).

367

368 **TA12 prevents BoNT/A1 interaction with SV2C-LD**

369 The HDX-defined TA12 epitope overlaps with the SV2C-LD and the GT1b binding sites
370 identified by X-ray crystallography (6, 40). SV2C-LD and GT1b both correspond to the
371 neuronal cell surface receptors used by BoNT/A to efficiently and specifically enter neurons
372 via a synergetic dual-binding process (8, 46-48). Based on this observation, we hypothesized that
373 TA12 binding might interfere with the interaction of both SV2C-LD and GT1b.

374 We first focused our attention on the H_{CA1}:SV2C-LD interaction. The deuterium uptake
375 profil of H_{CA1} was monitored in the SV2C-LD:H_{CA1} complex and compared to the one
376 obtained in the presence of TA12. The binding of SV2C-LD induced several statistically
377 significant changes (Wald test, $p < 0.05$) in deuterium uptake in H_{CA1} (**Figure 2A; Extended**
378 **Figures 4B, 5**). As observed in the H_{CA1}:TA12 complex, major reductions were observed in
379 region 2 of the H_{CC} domain (peptides 1145-1154 and 1148-1154, region 5 in **Figure 1**) covering
380 loops β 39- β 40 and β 40- β 41. Region 2 corresponds to the main SV2C-LD interaction site
381 identified by X-ray crystallography and contains critical residues for binding such as T1145
382 and T1146 (**Figures 2B**) (6, 10). Therefore, these data confirm that TA12 and SV2C both target
383 a common binding region on H_{CA1} (Compare **Figures 1A, 1B and 2A, 2B**). Two additional
384 regions surrounding residues 1145-1154, namely region 1 (peptides 946-955, 946-958 and 946-
385 961) in the H_{CN} domain and region 3 (peptides 1282-1296, 1283-1296, 1284-1296 and 1285-
386 1296) in the C-terminal part of H_{CC}, also display minor but statistically significant reductions
387 in uptake upon complex formation. Region 3 contains several overlapping peptides with similar
388 back-exchange values (**Extended file HDX.xls**) allowing to confine the effects of SV2C-LD
389 binding to segment 1285-1296 *only*. This segment contains residue R1294 involved in the
390 interaction and the binding specificity with SV2C-LD. Finally, although region 1 is very close
391 to the main SV2C-LD interaction site (i.e., region 2), this latter was not identified as part of the
392 SV2C-LD binding interface by X-ray crystallography (**Figure 2B**). Based on this observation,
393 the slight decrease in solvent accessibility observed in 946-961 might be attributed to a change
394 in dynamics rather than a masking effect.

395 We next performed *in vitro* experiments to analyze the interference of TA12 on the binding
396 of recombinant H_{CA1} to SV2C-LD immobilized on glutathione-Sepharose 4B beads. As shown
397 in **Figure 2C**, H_{CA1} binding to immobilized SV2C-LD was prevented in a TA12 dose-

398 dependent manner. More than 90% inhibition of binding was obtained at an equimolar ratio
399 between TA12 and H_CA1. These results confirm that TA12 prevents the formation of the
400 toxin/receptor complex via direct interaction with H_CA1. Thus, as observed with the
401 neutralizing ciA-C2 VHH, TA12 blocks the entry of BoNT/A1 into neuronal cells by targeting
402 one critical area of the toxin-cell receptor interface.

403

404 **TA12 affects H_CA1 binding to GT1b**

405 We next focused our attention on the H_CA1:GT1b interaction. Our HDX-MS data shows
406 that TA12 affects the solvent accessibility of elements involved in the GT1b-binding site
407 (**Figure 3A**). Region 1116-1124 contains residue Y1117 which directly coordinates GT1b
408 through hydrogen bondings with sialic acid 5 (Sia5); residue F1252 in region 1250-1252 also
409 hydrogen bonds to galactose 4 (Gal4) of the GT1b ganglioside (40). Compared to SV2C-LD,
410 GT1b only shares a limited overlapping binding area with TA12 on H_CA1 (**Figure 3A**).
411 Therefore, TA12 is not expected to directly compete with GT1b binding on H_CA1 as observed
412 with SV2C-LD but rather to affect the H_CA1:GT1b interaction mainly through steric clashes.

413 To determine the effects of TA12 on H_CA1 binding to GT1b, an inhibition binding assay
414 was performed using GT1b coated on plastic plate and incubated with H_CA1 either alone or in
415 the presence of TA12. As shown in Figure 3B, increased concentrations of TA12 result in
416 inhibition of H_CA1 binding to GT1b. Complete inhibition of H_CA1 binding to GT1b was
417 achieved at a much higher TA12/H_CA1 molar ratio compared to SV2C-LD (10:1 for GT1b; 1:1
418 for SV2C-LD), hence suggesting that TA12 mainly causes indirect interferences with GT1b.
419 Altogether, these data confirm that TA12 is also able to interfere with H_CA1 binding to GT1b
420 albeit with a lower efficiency compared to the binding inhibition of H_CA1 to SV2C-LD.

421

422 **Residue N1006 is important for TA12 binding.**

423 Although TA12 recognizes the H_C domain of BoNT/A subtypes with high affinity (i.e., in
424 the low pM-nM range; **Table 2**), the efficiency of neutralization appears subtype dependent.
425 The quantity of TA12 required to neutralize 50% of the activity of both BoNT/A5 and A7
426 appears 400- and 40-fold higher than for BoNT/A1, respectively (**Table 1**). Interestingly, the
427 H_C domain of BoNT/A1 shares respectively 94.1 and 91.7% sequence identity with H_CA5 and
428 H_CA7, suggesting that small variations in the primary sequence are sufficient to explain the
429 difference of neutralizing potency by TA12. To test this hypothesis, specific residues mainly
430 positioned within the HDX-MS defined TA12 epitope where major changes in deuterium
431 uptake occur upon binding were selected for substitution (**Extended Figure 6**). Four distinct

432 residues of H_CA1 including N1006 (region 2, **Figure 1**), and V1143, M1144 and R1156 (region
433 5, **Figure 1**) were replaced by the corresponding residues found in H_CA5 or H_CA7. The
434 modified residues correspond to natural H_C variants and their mutation is therefore not expected
435 to cause any local secondary structural changes on H_CA1. The substitution of V1143 alone or
436 in combination with M1144 and R1156 showed no significant effect on TA12 binding (**Table**
437 **2**). By contrast, the substitution of N1006 with alanine strongly affects the binding of TA12 to
438 H_CA1 with a 280-fold reduction in affinity compared to wild type (**Table 2**) confirming the
439 importance of N1006 in complex formation.

440

441 **DISCUSSION**

442 Neutralizing antibodies against BoNT represent the only available antidote against
443 botulism considering that vaccination is not an appropriate strategy due to the expanding
444 therapeutic applications of BoNTs. Although equine anti-BoNT polyclonal sera are able to
445 efficiently neutralize all seven known BoNT toxinotypes, their use can cause dramatic side
446 effects (13, 49-53). Alternative therapeutic antitoxin approaches, such as mAbs or peptide
447 inhibitors (6), are currently explored to reduce the risks of serum sickness and cardiac arrest.
448 Human anti-BoNT immune globulins obtained from vaccinated donors have been developed
449 for the treatment of infant botulism, but their production is not easily scalable (14).
450 Recombinant mAbs and more specially recombinant humanized mAbs represent a promising
451 and safer alternative strategy for botulism treatment. Their production is highly reproducible
452 compared to animal hyperimmune sera thereby preventing batch to batch variations in antibody
453 affinity (50). Over the last decade, several neutralizing mAbs against the distinct BoNT types
454 have been generated (17, 18, 54). However, mAbs are specific of single epitopes *only* and
455 extended protective coverage most often requires the combination of several mAbs. For
456 example, the association of three distinct mAbs targeting non-overlapping epitopes of BoNT/A
457 was found to be highly protective, whereas each single mAb showed no significant protection.
458 Moreover, the three mAb in combination induced a 90-fold greater neutralizing potency of
459 BoNT/A than human hyperimmune globulins (21). Although effective to treat botulism, the
460 association of several mAbs introduces unique development and manufacturing challenges for
461 clinical application. Recently, a single tri-epitopic IgG1-based mAb (TeAb) containing the
462 binding sites of three individual anti-BoNT/A1 mAbs was engineered (22). TeAb was found to
463 be much more potent in mouse-neutralization assay than any of the three single mAbs and
464 almost as potent as the combination of the three individual mAbs against BoNT/A1. Though

465 the neutralization potency of TeAb against the other BoNT/A subtypes was not reported, this
466 work highlights the potential of using single mAbs as alternative antitoxin solution (22).

467

468 In this study, we showed that the single TA12 mAb raised against H_CA1 is a potent
469 inhibitor of the two most frequent subtypes involved in human botulism, namely A1 and A2
470 (55-57), but also A3. TA12 recognizes a conformational epitope mainly composed of solvent
471 accessible loops located at the interface between the H_{CN} and the H_{CC} subdomain. The TA12
472 binding site overlaps with both the SV2C and the GT1b binding interfaces on H_CA1, causing
473 interferences with the interaction of the two neuronal cell surface receptors used by BoNT/A to
474 enter neurons. The strong neutralization potency of TA12 is therefore achieved by the
475 synergetic and simultaneous inhibition of BoNT/A binding to GT1b and the peptide moiety of
476 the SV2C luminal domain.

477 Two additional BoNT/A neutralizing antibodies have been reported to block the
478 recognition of SV2C: the camelid single domain ciA-C2 antibody (42, 43) and the human
479 monoclonal antibody CR1 currently in clinical trials (44, 45). The identification of the TA12
480 binding site provides a means to compare the different epitopes on H_CA1 and the neutralization
481 mechanism of each antibody. All three antibodies target the same H_{CN}/H_{CC} junction, which was
482 shown to elicit neutralizing antibodies against BoNT/A (28), but they adopt distinct orientation
483 on H_CA1 (**Figure 4**). CR1 mainly occupies the SV2C glycan binding site on the H_{CN}
484 subdomain. The CR1 epitope locates on the same H_CA1's face than the glycosylated SV2C
485 (gSV2C) without sharing any overlapping peptide regions with gSV2C. The large size of CR1
486 and its close proximity with gSV2C are sufficient to generate local steric clashes between
487 portions of CR1 and gSV2C, causing indirect interferences with gSV2C binding on H_CA1 (10,
488 45). The strong neutralizing potency of CR1 is therefore driven by two simultaneous blocking
489 effects: an indirect effect with the SV2C peptides moieties and a direct effect through the
490 occupation of the SV2C glycan binding site. As observed with CR1, ciA-C2 largely occupies
491 the binding site for the SV2C glycan but it also interacts with a key region in the H_{CN} subdomain
492 containing critical residues for gSV2C binding (**Figure 4**). Thus, ciA-C2 simultaneously
493 inhibits both the protein- and the glycan- interactions between BoNT/A1 and gSV2C via direct
494 blocking effects (43). The TA12 epitope shares common structural features with ciA-C2 as they
495 both occupy the same gSV2C peptide binding site on H_CA1 and directly block gSV2C binding
496 to BoNT/A (**Figure 4**). However, the TA12 binding interface lies on the face opposite
497 recognized by both ciA-C2 and CR1, confirming that the H_{CN}/H_{CC} junction contains distinct
498 antigenic regions able to elicit highly potent and unique BoNT/A neutralizing antibodies (28).

499 In contrast to both ciA-C2 and CR1, TA12 does not compete with the SV2C glycan but
500 interferes with H_CA1 binding to GT1b.

501 The identification of the TA12 epitope on BoNT/A also provides a means to understand
502 the variations in potency observed with the different H_CA subtypes (**Tables 1, 2**). The three
503 main regions defining the TA12 epitope (i.e., I1005-D1009, Y1117-V1125, and L1136-L1154;
504 **Extended Figure 6**) are relatively well conserved hence explaining the capabilities of TA12 to
505 recognize all H_CA subtypes with high affinity. As previously reported, the antitoxin efficacy of
506 antibodies largely depends on their binding affinity (42). Thereby, the highest TA12 binding
507 affinities and neutralization potencies were obtained with subtypes A1, A3 and A2 whereas the
508 lowest were observed with A5 and A7. TA12 binds A5 and A7 with affinity values comparable
509 to both ciA-C2 and CR1 (i.e., in the low nanomolar range), and yet only poorly neutralizes
510 BoNT/A5 in the mouse lethality assay. Low nanomolar K_D are therefore not sufficient because
511 TA12 interferes simultaneously with the two BoNT/A cell binding partners. The unique
512 neutralization mechanism of TA12 requires therefore low picomolar range affinity to prevent
513 the displacement of the bound antibody from the toxin by either gSV2C, GT1b or both. We
514 believe therefore that the differences in potency observed between H_CA subtypes are due to
515 subtle amino-acid changes within the TA12 binding interface, resulting in lower K_D values, as
516 we showed with residue 1006 in H_CA5. In addition, TA12 interferes on H_CA1 interaction with
517 gangliosides. Albeit TA12 prevented H_CA1 binding to GT1b with lower efficiency compared
518 to SV2C-LD, the cumulative effect of TA12 on binding to both types of H_CA1 cell receptors
519 likely contributes to the highly efficient *in vivo* neutralization observed in mouse protection
520 assay. To our knowledge, TA12 is the first antibody able to neutralize BoNT/A by
521 simultaneously interfering with the binding to the two cell surface receptor types on
522 motoneurons.

523

524 **Acknowledgements**

525 We thank UtechS MSBio of Institut Pasteur for the access to the HDX-MS instrumentation.
526 The CACSICE Equipex ANR-11-EQPX-0008 is acknowledged.

527

528 **Author contributions**

529 M.R.P. designed the project. S.B., M.R.P, CRE, AW, SS, MM, designed and performed the
530 experiments. S.B., M.R.P and CRE analyzed the data. S.B. and M.R.P. wrote the manuscript.
531 All authors discussed and commented on the manuscript.

532

533

534 **REFERENCES**

535

- 536 1. Peck, M. W., Smith, T. J., Anniballi, F., Austin, J. W., Bano, L., Bradshaw, M., Cuervo,
537 P., Cheng, L. W., Derman, Y., Dorner, B. G., Fisher, A., Hill, K. K., Kalb, S. R.,
538 Korkeala, H., Lindstrom, M., Lista, F., Luquez, C., Mazuet, C., Pirazzini, M., Popoff, M.
539 R., Rossetto, O., Rummel, A., Sesardic, D., Singh, B. R., and Stringer, S. C. (2017)
540 Historical Perspectives and Guidelines for Botulinum Neurotoxin Subtype Nomenclature.
541 *Toxins (Basel)* **9**, 38
- 542 2. Poulain, B., and Popoff, M. R. (2019) Why Are Botulinum Neurotoxin-Producing
543 Bacteria So Diverse and Botulinum Neurotoxins So Toxic? *Toxins (Basel)*. **11(1)**.
544 toxins11010034. doi: 11010010.11013390/toxins11010034.
- 545 3. Arnon, S. S., Schechter, R., Inglesby, T. V., Henderson, D. A., Bartlett, J. G., Ascher, M.
546 S., Eitzen, E., Fine, A. D., Hauer, J., Layton, M., Lillibridge, S., Osterholm, M. T.,
547 O'Toole, T., Parker, G., Perl, T. M., Russell, P. K., Swerdlow, D. L., and Tonat, K.
548 (2001) Botulinum toxin as a biological weapon: medical and public health management.
549 *JAMA* **285**, 1059-1070
- 550 4. Poulain, B., Molgo, J., and Popoff, M. R. (2015) Clostridial neurotoxins: from the
551 cellular and molecular mode of action to their therapeutic use. In *The Comprehensive*
552 *Sourcebook of Bacterial Protein Toxins* (Alouf, J., Ladant, D., and Popoff, M. R., eds)
553 pp. 287-336, Elsevier, Amsterdam
- 554 5. Rossetto, O., Pirazzini, M., and Montecucco, C. (2014) Botulinum neurotoxins: genetic,
555 structural and mechanistic insights. *Nat Rev Microbiol*. **12**, 535-549. doi:
556 10.1038/nrmicro3295.
- 557 6. Benoit, R. M., Frey, D., Hilbert, M., Kevenaar, J. T., Wieser, M. M., Stirnimann, C. U.,
558 McMillan, D., Ceska, T., Lebon, F., Jaussi, R., Steinmetz, M. O., Schertler, G. F.,
559 Hoogenraad, C. C., Capitani, G., and Kammerer, R. A. (2014) Structural basis for
560 recognition of synaptic vesicle protein 2C by botulinum neurotoxin A. *Nature*. **505**, 108-
561 111. doi: 10.1038/nature12732.
- 562 7. Dong, M., Liu, H., Tepp, W. H., Johnson, E. A., Janz, R., and Chapman, E. R. (2008)
563 Glycosylated SV2A and SV2B mediate the entry of botulinum neurotoxin E into neurons.
564 *Mol Biol Cell* **19**, 5226-5237

- 565 8. Mahrhold, S., Rummel, A., Bigalke, H., Davletov, B., and Binz, T. (2006) The synaptic
566 vesicle protein 2C mediates the uptake of botulinum neurotoxin A into phrenic nerves.
567 *FEBS Lett* **580**, 2011-2014
- 568 9. Rummel, A., Mahrhold, S., Bigalke, H., and Binz, T. (2004) The H_{cc}-domain of
569 botulinum neurotoxins A and B exhibits a singular ganglioside binding site displaying
570 serotype specific carbohydrate interaction. *Mol. Microbiol.* **51**, 631-643
- 571 10. Yao, G., Zhang, S., Mahrhold, S., Lam, K. H., Stern, D., Bagramyan, K., Perry, K.,
572 Kalkum, M., Rummel, A., Dong, M., and Jin, R. (2016) N-linked glycosylation of SV2 is
573 required for binding and uptake of botulinum neurotoxin A. *Nat Struct Mol Biol* **23**, 656-
574 662
- 575 11. Yowler, B. C., Kensinger, R. D., and Schengrund, C. L. (2002) Botulinum neurotoxin A
576 activity is dependent upon the presence of specific gangliosides in neuroblastoma cells
577 expressing synaptotagmin I. *J. Biol. Chem.* **277**, 32815-32819
- 578 12. Black, R. E., and Gunn, R. A. (1980) Hypersensitivity reactions associated with botulinal
579 antitoxin. *Am J Med.* **69**, 567-570. doi: 510.1016/0002-9343(1080)90469-90466.
- 580 13. Schussler, E., Sobel, J., Hsu, J., Yu, P., Meaney-Delman, D., Grammer, L. C., 3rd, and
581 Nowak-Wegrzyn, A. (2017) Workgroup Report by the Joint Task Force Involving
582 American Academy of Allergy, Asthma & Immunology (AAAAI); Food Allergy,
583 Anaphylaxis, Dermatology and Drug Allergy (FADDA) (Adverse Reactions to Foods
584 Committee and Adverse Reactions to Drugs, Biologicals, and Latex Committee); and the
585 Centers for Disease Control and Prevention Botulism Clinical Treatment Guidelines
586 Workgroup-Allergic Reactions to Botulinum Antitoxin: A Systematic Review. *Clin Infect*
587 *Dis.* **66**, S65-S72. doi: 10.1093/cid/cix1827.
- 588 14. Arnon, S. S., Schechter, R., Maslanka, S. E., Jewell, N. P., and Hatheway, C. L. (2006)
589 Human botulism immune globulin for the treatment of infant botulism. *N Engl J Med*
590 **354**, 462-471
- 591 15. Khouri, J. M., Motter, R. N., and Arnon, S. S. (2018) Safety and immunogenicity of
592 investigational recombinant botulinum vaccine, rBV A/B, in volunteers with pre-existing
593 botulinum toxoid immunity. *Vaccine.* **36**, 2041-2048. doi:
594 2010.1016/j.vaccine.2018.2002.2042.
- 595 16. Nayak, S. U., Griffiss, J. M., McKenzie, R., Fuchs, E. J., Jurao, R. A., An, A. T., Ahene,
596 A., Tomic, M., Hendrix, C. W., and Zenilman, J. M. (2014) Safety and pharmacokinetics
597 of XOMA 3AB, a novel mixture of three monoclonal antibodies against botulinum toxin
598 A. *Antimicrob Agents Chemother.* **58**, 5047-5053. doi: 5010.1128/AAC.02830-02814.

- 599 17. Rasetti-Escargueil, C., Avril, A., Miethe, S., Mazuet, C., Derman, Y., Selby, K., Thullier,
600 P., Pelat, T., Urbain, R., Fontayne, A., Korkeala, H., Sesardic, D., Hust, M., and Popoff,
601 M. R. (2017) The European AntibotABE Framework Program and Its Update:
602 Development of Innovative Botulinum Antibodies. *Toxins (Basel)* **9**, 309. doi:
603 10.3390/toxins9100309
- 604 18. Lou, J., and Marks, J. D. (2018) Botulinum Neurotoxins (BoNTs)-Antibody and Vaccine.
605 *Toxins (Basel)*. **10(12)**. toxins10120495. doi: 10120410.10123390/toxins10120495.
- 606 19. Fan, Y., Garcia-Rodriguez, C., Lou, J., Wen, W., Conrad, F., Zhai, W., Smith, T. J.,
607 Smith, L. A., and Marks, J. D. (2017) A three monoclonal antibody combination potently
608 neutralizes multiple botulinum neurotoxin serotype F subtypes. *PLoS One* **12**, e0174187
- 609 20. Garcia-Rodriguez, C., Razai, A., Geren, I. N., Lou, J., Conrad, F., Wen, W. H., Farr-
610 Jones, S., Smith, T. J., Brown, J. L., Skerry, J. C., Smith, L. A., and Marks, J. D. (2018)
611 A Three Monoclonal Antibody Combination Potently Neutralizes Multiple Botulinum
612 Neurotoxin Serotype E Subtypes. *Toxins (Basel)* **10**, doi: 10.3390/toxins10030105
- 613 21. Nowakowski, A., Wang, C., Powers, D. B., Amersdorfer, P., Smith, T. J., Montgomery,
614 V. A., Sheridan, R., Blake, R., Smith, L. A., and Marks, J. D. (2002) Potent neutralization
615 of botulinum neurotoxin by recombinant oligoclonal antibody. *Proc. Ntl. Acad. Sci.*
616 *(USA)* **99**, 11346-11350
- 617 22. Lou, J., Wen, W., Conrad, F., Meng, Q., Dong, J., Sun, Z., Garcia-Rodriguez, C., Farr-
618 Jones, S., Cheng, L. W., Henderson, T. D., Brown, J. L., Smith, T. J., Smith, L. A.,
619 Cormier, A., and Marks, J. D. (2018) A Single Tri-Epitopic Antibody Virtually
620 Recapitulates the Potency of a Combination of Three Monoclonal Antibodies in
621 Neutralization of Botulinum Neurotoxin Serotype A. *Toxins (Basel)* **10**, 84. doi:
622 10.3390/toxins10020084
- 623 23. Mazuet, C., Dano, J., Popoff, M. R., Creminon, C., and Volland, H. (2010)
624 Characterization of botulinum neurotoxin type A neutralizing monoclonal antibodies and
625 influence of their half-lives on therapeutic activity. *PLoS One* **5**, e12416
- 626 24. Prigent, J., Mazuet, C., Boquet, D., Lamourette, P., Volland, H., Popoff, M. R.,
627 Creminon, C., and Simon, S. (2010) Production and characterisation of a neutralising
628 chimeric antibody against botulinum neurotoxin A. *PLoS One* **5**, e13245
- 629 25. Brier, S., Le Mignon, M., Jain, K., Lebrun, C., Peurois, F., Kellenberger, C., Bordas-Le
630 Floch, V., Mascarell, L., Nony, E., and Moingeon, P. (2018) Characterization of epitope
631 specificities of reference antibodies used for the quantification of the birch pollen
632 allergen Bet v 1. *Allergy*. **73**, 1032-1040. doi: 1010.1111/all.13364.

- 633 26. Brier, S., Lemaire, D., DeBonis, S., Kozielski, F., and Forest, E. (2006) Use of
634 hydrogen/deuterium exchange mass spectrometry and mutagenesis as a tool to identify
635 the binding region of inhibitors targeting the human mitotic kinesin Eg5. *Rapid Commun*
636 *Mass Spectrom* **20**, 456-462. doi: 410.1002/rcm.2329.
- 637 27. Volland, H., Lamourette, P., Nevers, M. C., Mazuet, C., Ezan, E., Neuburger, L. M.,
638 Popoff, M., and Creminon, C. (2008) A sensitive sandwich enzyme immunoassay for free
639 or complexed *Clostridium botulinum* neurotoxin type A. *J Immunol Methods* **330**, 120-
640 129
- 641 28. Tavallaie, M., Chenal, A., Gillet, D., Pereira, Y., Manich, M., Gibert, M., Raffestin, S.,
642 Popoff, M. R., and Marvaud, J. C. (2004) Interaction between the two subdomains of the
643 C-terminal part of the botulinum neurotoxin A is essential for the generation of protective
644 antibodies. *FEBS Lett.* **572**, 299-306
- 645 29. Couesnon, A., Molgo, J., Connan, C., and Popoff, M. R. (2012) Preferential entry of
646 botulinum neurotoxin A Hc domain through intestinal crypt cells and targeting to
647 cholinergic neurons of the mouse intestine. *PLoS Pathog* **8**, e1002583
- 648 30. Burns, J. R., Lambert, G. S., and Baldwin, M. R. (2017) Insights into the Mechanisms by
649 Which Clostridial Neurotoxins Discriminate between Gangliosides. *Biochemistry.* **56**,
650 2571-2583. doi: 2510.1021/acs.biochem.2576b01246.
- 651 31. Karalewitz, A. P., Kroken, A. R., Fu, Z., Baldwin, M. R., Kim, J. J., and Barbieri, J. T.
652 (2010) Identification of a unique ganglioside binding loop within botulinum neurotoxins
653 C and D-SA. *Biochemistry* **49**, 8117-8126
- 654 32. Strotmeier, J., Gu, S., Jutzi, S., Mahrhold, S., Zhou, J., Pich, A., Eichner, T., Bigalke, H.,
655 Rummel, A., Jin, R., and Binz, T. (2011) The biological activity of botulinum neurotoxin
656 type C is dependent upon novel types of ganglioside binding sites. *Mol Microbiol* **81**,
657 143-156
- 658 33. Malizio, C. J., Goodnough, M. C., and Johnson, E. A. (2000) Purification of *Clostridium*
659 *botulinum* type A neurotoxin. *Methods Mol Biol* **145**, 27-39
- 660 34. Rasetti-Escargueil, C., Avril, A., Chahboun, S., Tierney, R., Bak, N., Miethe, S., Mazuet,
661 C., Popoff, M. R., Thullier, P., Hust, M., Pelat, T., and Sesardic, D. (2015) Development
662 of human-like scFv-Fc antibodies neutralizing Botulinum toxin serotype B. *MAbs* **7**,
663 1161-1177
- 664 35. Masson, G. R., Burke, J. E., Ahn, N. G., Anand, G. S., Borchers, C., Brier, S., Bou-Assaf,
665 G. M., Engen, J. R., Englander, S. W., Faber, J., Garlish, R., Griffin, P. R., Gross, M. L.,
666 Guttman, M., Hamuro, Y., Heck, A. J. R., Houde, D., Iacob, R. E., Jorgensen, T. J. D.,

- 667 Kaltashov, I. A., Klinman, J. P., Konermann, L., Man, P., Mayne, L., Pascal, B. D.,
668 Reichmann, D., Skehel, M., Snijder, J., Strutzenberg, T. S., Underbakke, E. S., Wagner,
669 C., Wales, T. E., Walters, B. T., Weis, D. D., Wilson, D. J., Wintrode, P. L., Zhang, Z.,
670 Zheng, J., Schriemer, D. C., and Rand, K. D. (2019) Recommendations for performing,
671 interpreting and reporting hydrogen deuterium exchange mass spectrometry (HDX-MS)
672 experiments. *Nat Methods*. **16**, 595-602. doi: 510.1038/s41592-41019-40459-y.
- 673 36. Hourdel, V., Volant, S., O'Brien, D. P., Chenal, A., Chamot-Rooke, J., Dillies, M. A., and
674 Brier, S. (2016) MEMHDX: an interactive tool to expedite the statistical validation and
675 visualization of large HDX-MS datasets. *Bioinformatics*. **32**, 3413-3419. doi:
676 3410.1093/bioinformatics/btw3420. Epub 2016 Jul 3413.
- 677 37. Guttman, M., Weis, D. D., Engen, J. R., and Lee, K. K. (2013) Analysis of overlapped
678 and noisy hydrogen/deuterium exchange mass spectra. *J Am Soc Mass Spectrom*. **24**,
679 1906-1912. doi: 1910.1007/s13361-13013-10727-13365.
- 680 38. Pellett, S., Tepp, W. H., Whitmarsh, R. C., Bradshaw, M., and Johnson, E. A. (2015) In
681 vivo onset and duration of action varies for botulinum neurotoxin A subtypes 1-5.
682 *Toxicon* **107**, 37-42
- 683 39. Whitmarsh, R. C., Tepp, W. H., Bradshaw, M., Lin, G., Pier, C. L., Scherf, J. M.,
684 Johnson, E. A., and Pellett, S. (2013) Characterization of botulinum neurotoxin A
685 subtypes 1 through 5 by investigation of activities in mice, in neuronal cell cultures, and
686 in vitro. *Infect Immun*. **81**, 3894-3902. doi: 3810.1128/IAI.00536-00513.
- 687 40. Stenmark, P., Dupuy, J., Imamura, A., Kiso, M., and Stevens, R. C. (2008) Crystal
688 structure of botulinum neurotoxin type A in complex with the cell surface co-receptor
689 GT1b-insight into the toxin-neuron interaction. *PLoS Pathog* **4**, e1000129
- 690 41. Guttman, M., Wales, T. E., Whittington, D., Engen, J. R., Brown, J. M., and Lee, K. K.
691 (2016) Tuning a High Transmission Ion Guide to Prevent Gas-Phase Proton Exchange
692 During H/D Exchange MS Analysis. *J Am Soc Mass Spectrom*. **27**, 662-668. doi:
693 610.1007/s13361-13015-11330-13368.
- 694 42. Mukherjee, J., Tremblay, J. M., Leysath, C. E., Ofori, K., Baldwin, K., Feng, X.,
695 Bedenice, D., Webb, R. P., Wright, P. M., Smith, L. A., Tzipori, S., and Shoemaker, C.
696 B. (2012) A novel strategy for development of recombinant antitoxin therapeutics tested
697 in a mouse botulism model. *PLoS One* **7**, e29941. doi:
698 29910.21371/journal.pone.0029941.

- 699 43. Yao, G., Lam, K. H., Weisemann, J., Peng, L., Krez, N., Perry, K., Shoemaker, C. B.,
700 Dong, M., Rummel, A., and Jin, R. (2017) A camelid single-domain antibody neutralizes
701 botulinum neurotoxin A by blocking host receptor binding. *Sci Rep* **7**, 7438
- 702 44. Garcia-Rodriguez, C., Geren, I. N., Lou, J., Conrad, F., Forsyth, C., Wen, W.,
703 Chakraborti, S., Zao, H., Manzanarez, G., Smith, T. J., Brown, J., Tepp, W. H., Liu, N.,
704 Wijesuriya, S., Tomic, M. T., Johnson, E. A., Smith, L. A., and Marks, J. D. (2011)
705 Neutralizing human monoclonal antibodies binding multiple serotypes of botulinum
706 neurotoxin. *Protein Eng Des Sel.* **24**, 321-331. doi: 310.1093/protein/gzq1111.
- 707 45. Garcia-Rodriguez, C., Levy, R., Arndt, J. W., Forsyth, C. M., Razai, A., Lou, J., Geren,
708 I., Stevens, R. C., and Marks, J. D. (2007) Molecular evolution of antibody cross-
709 reactivity for two subtypes of type A botulinum neurotoxin. *Nat Biotechnol.* **25**, 107-116.
710 doi: 110.1038/nbt1269.
- 711 46. Dong, M., Yeh, F., Tepp, W. H., Dean, C., Johnson, E. A., Janz, R., and Chapman, E. R.
712 (2006) SV2 Is the Protein Receptor for Botulinum Neurotoxin A. *Science* **312**, 592-596
- 713 47. Kozaki, S., Kamata, Y., Watarai, S., Nishiki, T., and Mochida, S. (1998) Ganglioside
714 GT1b as a complementary receptor component for *Clostridium botulinum* neurotoxins.
715 *Microbiol. Pathol.* **25**, 91-99
- 716 48. Yowler, B. C., and Schengrund, C. L. (2004) Botulinum neurotoxin A changes
717 conformation upon binding to ganglioside GT1b. *Biochemistry* **43**, 9725-9731
- 718 49. Hifumi, T., Yamamoto, A., Ato, M., Sawabe, K., Morokuma, K., Morine, N., Kondo, Y.,
719 Noda, E., Sakai, A., Takahashi, J., and Umezawa, K. (2017) Clinical Serum Therapy:
720 Benefits, Cautions, and Potential Applications. *Keio J Med.* **66**, 57-64. doi:
721 10.2302/kjm.2016-0017-IR.
- 722 50. Thanongsaksrikul, J., and Chaicumpa, W. (2011) Botulinum neurotoxins and botulism: a
723 novel therapeutic approach. *Toxins (Basel).* **3**, 469-488. doi: 410.3390/toxins3050469.
724 Epub 3052011 May 3050413.
- 725 51. Hill, S. E., Iqbal, R., Cadiz, C. L., and Le, J. (2013) Foodborne botulism treated with
726 heptavalent botulism antitoxin. *Ann Pharmacother.* **47**, e12. doi:
727 10.1345/aph.1341R1646.
- 728 52. Hibbs, R. G., Weber, J. T., Corwin, A., Allos, B. M., Abd el Rehim, M. S., Sharkawy, S.
729 E., Sarn, J. E., and McKee, K. T., Jr. (1996) Experience with the use of an investigational
730 F(ab')₂ heptavalent botulism immune globulin of equine origin during an outbreak of
731 type E botulism in Egypt. *Clin Infect Dis* **23**, 337-340

- 732 53. Yu, P. A., Lin, N. H., Mahon, B. E., Sobel, J., Yu, Y., Mody, R. K., Gu, W., Clements, J.,
733 Kim, H. J., and Rao, A. K. (2017) Safety and Improved Clinical Outcomes in Patients
734 Treated With New Equine-Derived Heptavalent Botulinum Antitoxin. *Clin Infect Dis.* **66**,
735 S57-S64. doi: 10.1093/cid/cix1816.
- 736 54. Marks, J. D. (2004) Deciphering antibody properties that lead to potent botulinum
737 neurotoxin neutralization. *Mov Disord* **19 Suppl 8**, S101-108
- 738 55. Carter, A. T., and Peck, M. W. (2015) Genomes, neurotoxins and biology of *Clostridium*
739 *botulinum* Group I and Group II. *Res Microbiol* **166**, 303-317
- 740 56. Mazuet, C., Legeay, C., Sautereau, J., Ma, L., Bouchier, C., Bouvet, P., and Popoff, M.
741 R. (2016) Diversity of Group I and II *Clostridium botulinum* Strains from France
742 Including Recently Identified Subtypes. *Genome Biol Evol* **8**, 1643-1660
- 743 57. Williamson, C. H., Sahl, J. W., Smith, T. J., Xie, G., Foley, B. T., Smith, L. A.,
744 Fernandez, R. A., Lindstrom, M., Korkeala, H., Keim, P., Foster, J., and Hill, K. (2016)
745 Comparative genomic analyses reveal broad diversity in botulinum-toxin-producing
746 Clostridia. *BMC Genomics* **17**, 180
747

748 **FIGURE LEGENDS**

749

750 **Figure 1 | Effects of TA12 binding on the deuterium uptake behavior of H_CA1.** **A,** The
751 fractional uptake difference plot was generated for each peptide and at each time point by
752 subtracting the deuterium uptake values in the TA12-unbound from those in the bound state.
753 Positive numbers indicate TA12-induced protection (regions 1, 2, 4, 5 and 6) while negative
754 values indicate an increase in solvent accessibility (region 3). The six regions displaying
755 statistically significant changes of deuterium uptake upon TA12 binding (Wald test, $p < 0.05$)
756 are highlighted in gray. Each dot corresponds to an average of three independent replicates. **B,**
757 Mapping of the HDX-MS results obtained after 60 min labeling onto the cartoon and surface
758 representations of H_CA1 (pdb # 2NZ9). The largest reductions of deuterium uptake mainly
759 occur within loops (regions 2, 4 and 5) located at the interface between the N-terminal lectin
760 subdomain (H_{CN}) and the C-terminal trefoil subdomain (H_{CC}) whereas changes in dynamics are
761 observed in H_{CN} *only*. “No change” refers to regions of H_CA1 that show no statistically
762 significant uptake difference between states during the time scale of the experiment. **C,** Mass
763 spectra and deuterium uptake plot of peptide 1017-1035 that displays a bimodal isotopic pattern
764 (EX1) in the presence of TA12. The EX1 behavior is characterized by an increase in the peak
765 width due to the overlap of two distinct isotopic distributions corresponding to the low (red)
766 and high (green) m/z populations. The center of these two distributions (blue, mix m/z) was
767 used to generate the fractional uptake difference values for peptide 1017-1035 (panel A).

768

769 **Figure 2 | TA12 blocks BoNT/A1 binding to SV2C-LD by targeting a common area on**
770 **H_CA1.** **A,** Effects of SV2C-LD binding on the deuterium uptake behavior of H_CA1. The
771 Fractional uptake difference plot was generated for each peptide and at each time point by
772 subtracting the uptake values measured in the SV2C-LD unbound-state from those in the bound
773 state. Positive numbers indicate SV2C-LD induced protection (regions 1, 2, and 3). Regions
774 displaying statistically significant changes of deuterium uptake upon SV2C-LD binding (Wald
775 test, $p < 0.05$) are highlighted in gray. Each dot corresponds to an average of three independent
776 replicates. **B,** Mapping of the HDX-MS results obtained after 60 min labeling onto the surface
777 representation of H_CA1 (pdb # 2NZ9). As observed with TA12, the largest reduction in
778 deuterium uptake occurs within region 2 (i.e., 1145-1154 corresponding to region 5 in **Figure**
779 **1A, 1B**). The position of the SV2C-LD binding site identified by X-ray crystallography is also
780 reported (magenta). The H_CA1 residues in direct interaction with SV2C-LD are indicated. “No
781 change” refers to regions of BoNT/A1 that show no statistically significant uptake difference

782 between states during the time scale of the experiment. **C**, Inhibition of H_CA1 binding to SV2C-
 783 LD by mAb TA12. H_CA1 (200 pmol) was preincubated with or without TA12 for 15 min at
 784 room temperature (Input) and then incubated with immobilized SV2C-LD on glutathione-
 785 Sepharose 4B beads for 90 min at 4°C. Bound H_CA1 was detected by 10% SDS-PAGE analysis
 786 after Coomassie blue staining. Load input volumes on gel were 1:10 of the total input volumes.
 787 TA12 was dissociated in heavy and light chains. A representative figure of 4 is shown.

788

789 **Figure 3 | Effects of TA12 on the binding of the GT1b ganglioside.** **A**, Structure of the
 790 H_CA1:GT1b complex (pdb # 2VU9) showing the position of the GT1b-binding site relative to
 791 the HDX-MS defined TA12 epitope. GT1b is shown as green sticks. A close-up view of the
 792 GT1b-binding interface is shown on the right side, where the position of residues Y1117 and
 793 F1252 involved in the coordination of GT1b are reported. The GT1b sialic acid 5 (Sia5) and
 794 galactose 4 (Gal4) hydrogen bonded respectively to Y1117 and F1252 are also indicated. The
 795 variations in deuterium uptake imposed by TA12 binding on H_CA1 are colored as in Figure 1.
 796 **B**, TA12 inhibition of H_CA1 binding to GT1b. H_CA1 (10 nM) was preincubated with or without
 797 increasing concentration of TA12 for 15 min at room temperature and then exposed to GT1b
 798 coated on 96-well plate (1 µg/well). Bound H_CA1 to GT1b was detected with rabbit anti- H_CA1
 799 antibodies and HRP-goat anti-rabbit IgG. Representative experiment in triplicate is shown.
 800 TA12 128 nM and above completely prevent the binding of H_CA1 (10 nM) to GT1b.

801

802 **Figure 4 | TA12 binds H_CA1 on the face opposite occupied by both ciA-C2 and the**
 803 **BoNT/A1-neutralizing therapeutic human monoclonal antibody CR1.** Superposition of the
 804 structures of the H_CA1:ciA-C2 (pdb # 5L21), H_CA1:CR1 (pdb # 2NYY), H_CA1:GT1b (pdb #
 805 2VU9) and H_CA1:gSV2C (pdb # 5JLV) complexes. GT1b and the N559-glycan of gSV2C are
 806 shown as green and cyan sticks respectively. CiA-C2 (dark red) partially occupies the binding
 807 site on H_CA1 of both the N-glycan (N559) and the peptide moieties of gSV2C, thereby
 808 interfering directly with gSV2C (cyan) binding to H_CA1. The region of H_CA1 containing
 809 critical residues for gSV2C binding (i.e., T1145 and T1146) and targeted by ciA-C2 is indicated
 810 by a black box. The BoNT/A1-neutralizing CR1 antibody (ribbon representation, gold) directly
 811 targets the gSV2C N599-glycan binding site on H_CA1 without competing with the gSV2C
 812 peptide binding site (black box). The variable region in the CR1 light chain overlaps almost
 813 completely with the ciA-C2 binding areas containing the gSV2C N599-glycan interaction site.
 814 The HDX-defined TA12 epitope (see color code in Figure 1) occupies the gSV2C peptide
 815 binding site targeted by ciA-C2 (black box), causing direct interferences with the peptide

816 moieties of gSV2C. In contrast to both ciA-C2 and CR1, TA12 does not affect the gSV2C
817 glycan binding region but recognize a region of the GT1b-binding site. Thus, TA12 partially
818 impaired H_cA1 binding to GT1b (Fig. 3B). The position of the TA12 epitope relative to the ciA-
819 C2, CR1 and gSV2C binding sites is better visualized using the H_cA1 surface representation
820 shown on the right side. TA12 shares a common binding interface with ciA-C2 but mainly
821 occupies the face opposite on H_cA1 to both ciA-C2 and CR1 (black circle). The position of the
822 N1006 residue identified as important for TA12 binding is indicated.

823

824

825

826 **Table 1.** Neutralization activity of TA12 mAb with BoNT/A subtypes827
828

TA12 mAb quantity (ng/mouse)	0	10,000	2,500	1,000	250	25	2.5	mAb quantity (ng/mouse) yielding 50% neutralization
BoNT/A1	6/6	0/2	/	0/4	1/7	4/10	6/6	2.5<25
BoNT/A2*	9/9	/	0/9	/	6/9	9/9	/	250
BoNT/A3*	9/9	/	0/9	/	0/9	6/9	/	25<250
BoNT/A5	6/6	5/8	4/4	8/8	5/5	2/2	/	1,000<10,000
BoNT/A7	6/6	1/6	5/6	5/8	8/8	2/2	/	250<1,000

829

830

831 mAb neutralization activity was determined using the mouse protection assay with estimated

832 5 MLD₅₀/mL of BoNT/A subtype and serial dilutions of mAb. 5 estimated MLD₅₀/mouse

833 were incubated with 2.5 to 10,000 ng of TA12 mAb for 30 min at room temperature and the

834 mixture (0.5 mL) was injected intraperitoneally into each mouse.

835 Results are expressed as the number of dead mice versus the total number of mice.

836 *Data from (23).

837

838
839**Table 2.** Binding affinities of mAb TA12 with BoNT/A subtypes H_C

BoNT/A H_C	Amino acid identity^a (%)	k_{on} (1/Ms)	k_{off} (1/s)	K_D (pM)
H _C A1	-	3.01 10 ⁵	7.1 10 ⁻⁶	23.6
H _C A2	87.0	6.96 10 ⁵	7.74 10 ⁻⁵	111
H _C A3	86.58	1.13 10 ⁶	6.58 10 ⁻⁵	58.1
H _C A4	91.76	2.13 10 ⁵	5.91 10 ⁻⁴	2780
H _C A5	94.11	7.95 10 ⁵	7.55 10 ⁻⁴	949
H _C A7	91.76	2.83 10 ⁵	5.94 10 ⁻⁴	2100
H _C A1 R1156M		4.79 10 ⁵	1.47 10 ⁻⁵	30.7
H _C A1 V1143I/M1144V		6.42 10 ⁵	5.63 10 ⁻⁶	8.77
H _C A1 V1143I/M1144V/R1156M		4.09 10 ⁵	4.61 10 ⁻⁵	113
H _C A1 N1006A		1.88 10 ⁵	1.27 10 ⁻³	6755

840

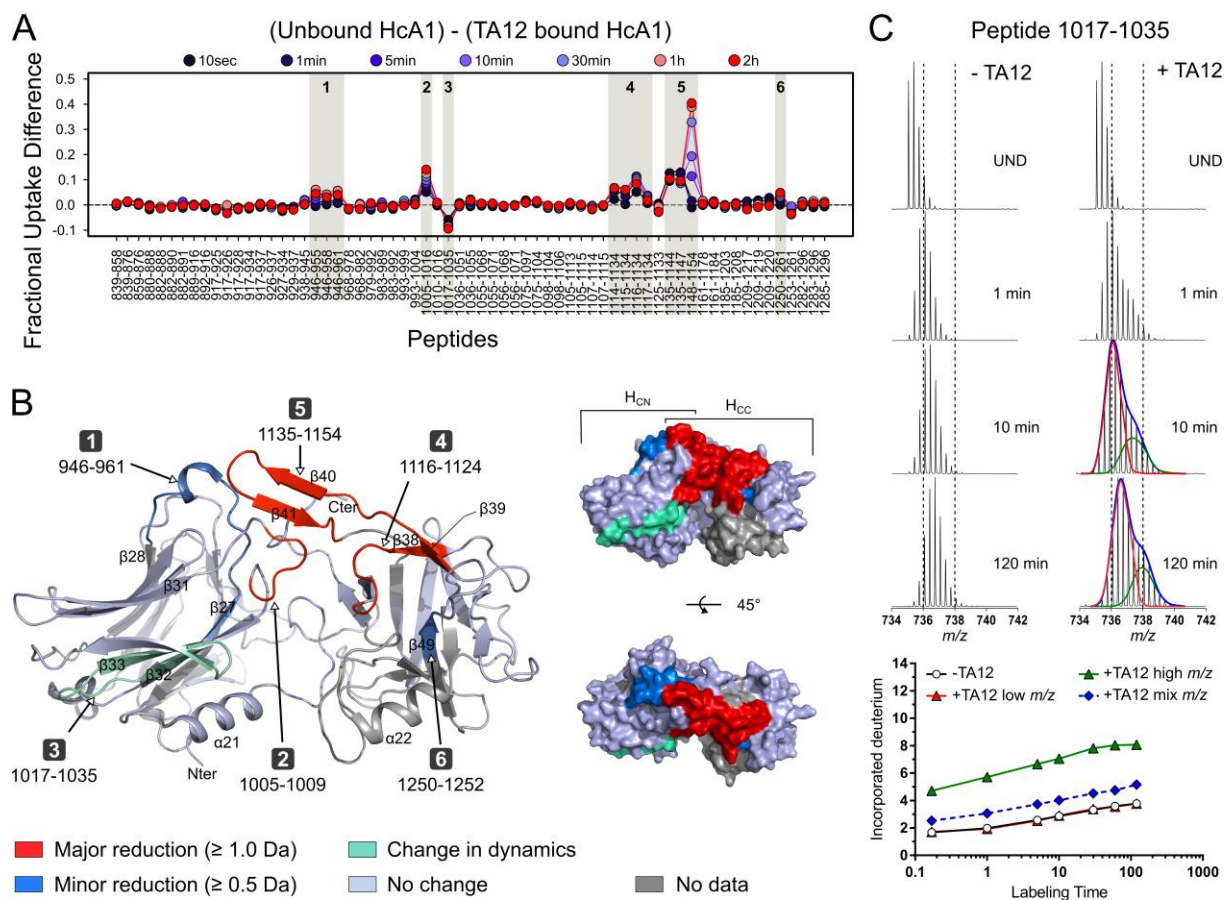
841 ^a Amino acid identity between H_CA1 and the other H_CA subtypes

842

843

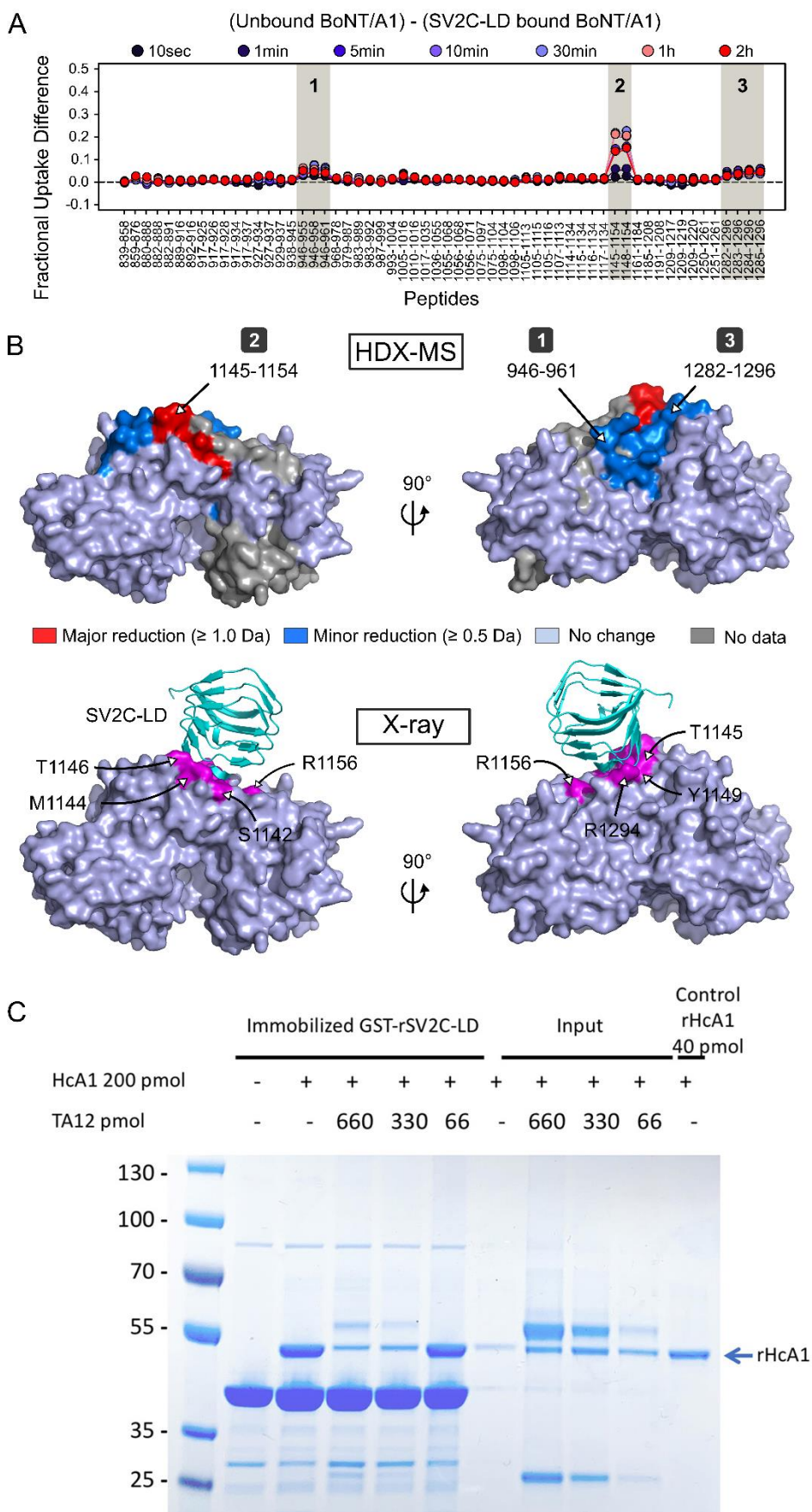
844

845 **Figure 1**
846



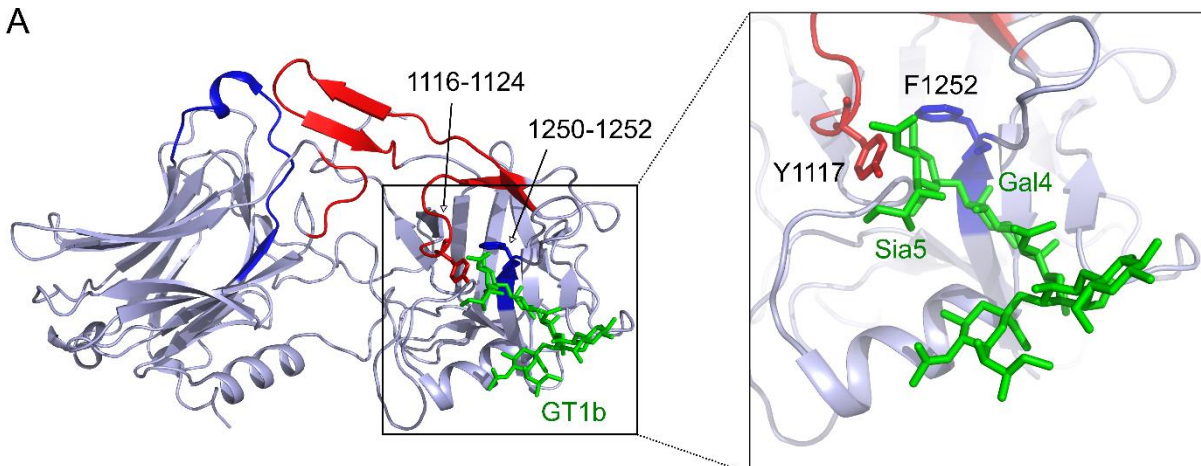
847
848

849 **Figure 2**
850

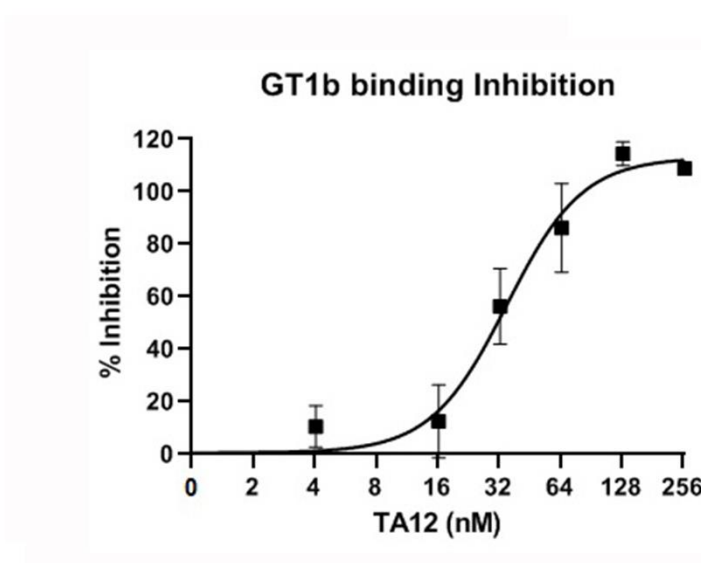


852 **Figure 3**
853

A

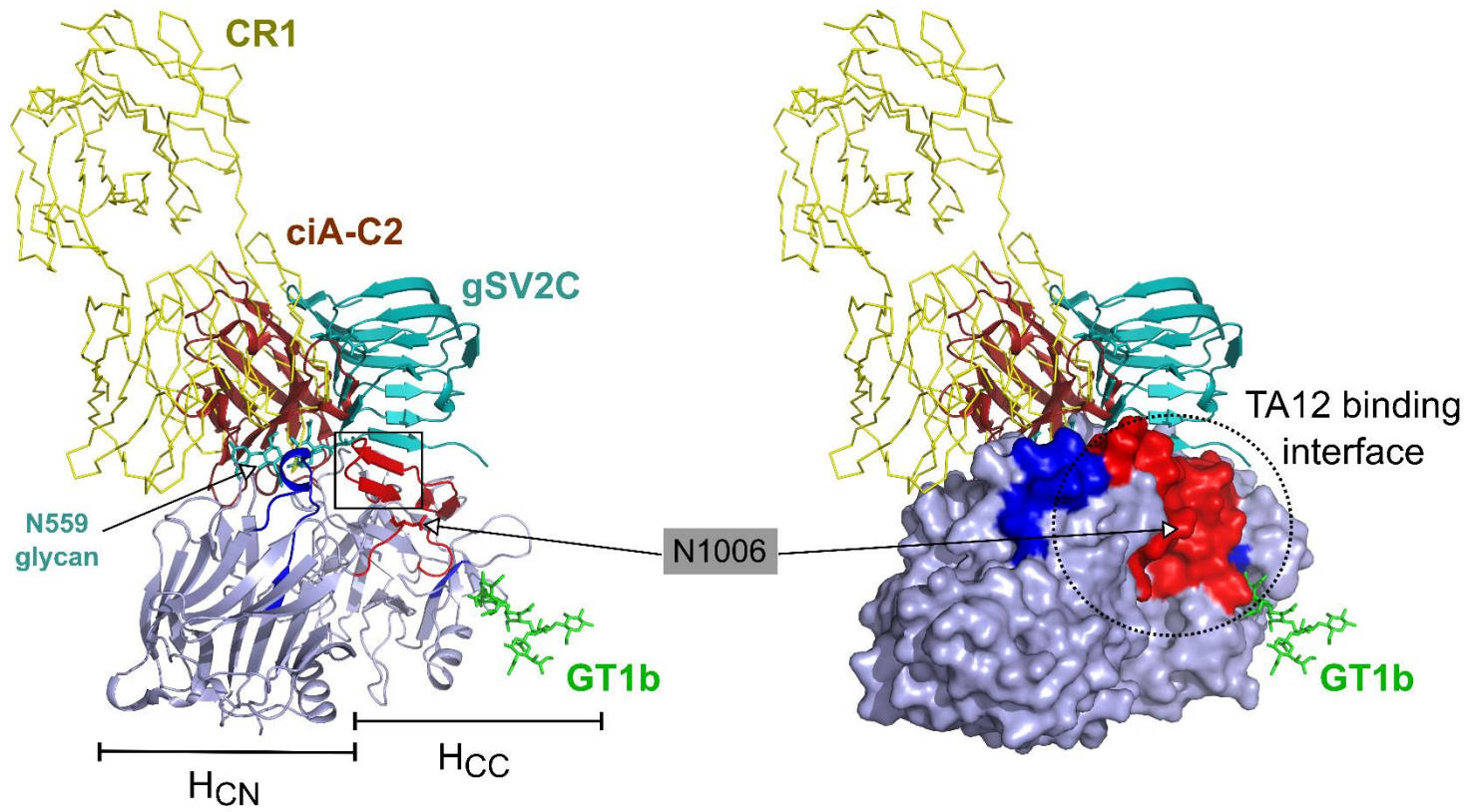


B



854

855 **Figure 4**
856



857